Langevin Equations for Fluctuating Surfaces

Alvin L.-S. Chua,* Christoph A. Haselwandter,† Chiara Baggio,‡ and Dimitri D. Vvedensky§
The Blackett Laboratory, Imperial College, London SW7 2BW, United Kingdom
(Dated: May 27, 2005)

Exact Langevin equations are derived for the height fluctuations of surfaces driven by the deposition of material from a molecular beam. We consider two types of model: deposition models, where growth proceeds by the deposition and instantaneous local relaxation of particles, with no subsequent movement, and models with concurrent random deposition and surface diffusion. Starting from a Chapman-Kolmogorov equation the deposition, relaxation, and hopping rules of these models are first expressed as transition rates within a master equation for the joint height probability density function. The Kramers-Moyal-van Kampen expansion of the master equation in terms of an appropriate "largeness" parameter yields, according to a limit theorem due to Kurtz [Stoch. Proc. Appl. **6**, 223 (1978)], a Fokker-Planck equation that embodies the statistical properties of the original lattice model. The statistical equivalence of this Fokker-Planck equation, solved in terms of its associated Langevin equation, and solutions of the Chapman-Kolmogorov equation, as determined by kinetic Monte Carlo (KMC) simulations of the lattice transition rules, is demonstrated explicitly by comparing the surface roughness and the lateral height correlations obtained from the two formulations for the Edwards-Wilkinson [Proc. Roy. Soc. London Ser. A **381**, 17 (1982)] and Wolf-Villain [Europhys. Lett. **13**, 389 (1990)] deposition models, and for a model with random deposition and surface diffusion. In each case, as the largeness parameter is increased, the Langevin equation converges to the surface roughness and lateral height correlations produced by KMC simulations for all times, including the crossover between different scaling regimes. We conclude by examining some of the wider implications of these results, including applications to heteroepitaxial systems and the passage to the continuum limit.

I. INTRODUCTION

The widespread application of lattice models to the basic phenomenology of epitaxial kinetics [1–3] has fostered a huge literature on the morphological evolution of fluctuating growth fronts [4–8] that has established these models as paradigms for driven nonequilibrium systems. One of the central concerns of this work is the expression of the time-development of a system, as determined by a set of transition rules between neighboring configurations, in terms of a stochastic differential equation. Several methods have been proposed for obtaining analytic formulations of rule-based lattice models, including phenomenological [9, 10] and symmetry [11–13] arguments, mappings onto other models [11, 14], real-space renormalization-group methods [15], and formal expansions of stochastic equations on a lattice [14, 16–19]. Although these studies have produced suggestive results for individual cases, a methodology that produces differential equations of motion for general lattice growth models has yet to be advanced.

An altogether different approach to associating a stochastic differential equation with a lattice model is based on the asymptotic scaling properties of the growth front. The shot noise of the deposition process causes kinetic roughening characterized by scale invariance analogous to that for dynamical critical phenomena near equilibrium [4]. The corresponding "critical" exponents are said to be universal if they depend only on the spatial dimension of the substrate and on the "relevant" terms in the equation of motion, rather than on microscopic details, such as the type of lattice or the spatial range of the transition rules. On this basis, several lattice models have been assigned to universality classes of particular Langevin equations [4, 5, 10, 20–26], although this can require extensive kinetic Monte Carlo (KMC) simulations to eliminate crossover effects [24–26]. But there are notable exceptions to this scenario. For such cases, a more fundamental approach to determining the continuum expressions of lattice models is required.

In this paper we develop a procedure for deriving *lattice* Langevin equations for the height fluctuations of driven surfaces that are statistically equivalent to KMC simulations [29]. We will focus on two basic model types: deposition models, where particles are deposited randomly, relax instantaneously to a neighboring site and remain there, and models with concurrent random deposition and surface diffusion. Examples of deposition models include random deposition, where the deposition site is the initial site, the Edwards-Wilkinson model [20, 30], where the deposition site is a local height minimum, the Wolf-Villain model [31, 32], where the deposition site is a local coordination maximum, and numerous variations thereon [33, 34]. Such relaxation rules model the short-range mobility of "hot" atoms deposited onto the surface by a molecular beam that is caused by the heat of condensation, especially near step edges, but are also used

*Institute of High Performance Computing, Singapore Science Park II, Singapore 117528.
†christoph.haselwandter@imperial.ac.uk
‡Present address: Instituut-Lorentz, Universiteit Leiden, P.O. Box 9506, 2300 RA Leiden, The Netherlands.
§d.vvedensky@imperial.ac.uk

to examine the effects of limited surface diffusion without incurring the computational overheads of a full hopping model.

KMC simulations of models with deposition and surface diffusion have explained many fundamental aspects of epitaxial phenomena through quantitative comparisons with experimental measurements, including growth on vicinal surfaces [2, 3], submonolayer island-size distributions [35–37], unstable growth [38, 39], and the role of multiple species in the growth of compound semiconductors [1, 40, 41]. Such simulations have the advantage of versatility and computational efficiency, but the absence of an underlying analytic formulation means that obtaining systematic results can be quite time consuming. Even ostensibly minor modifications to the transition rules necessitate performing an entire new set of simulations. One of the primary aims of the work reported here is to provide an analytic infrastructure to augment KMC simulations.

Our procedure begins by expressing the morphological evolution of a growth model as a Chapman-Kolmogorov equation for the joint conditional transition probability between height configurations of the system. Chapman-Kolmogorov equations and their associated master equations provide a complete statistical description of stochastic systems, but are amenable to direct analysis in only a few special cases [42–44]. KMC simulations provide a practical, albeit indirect, alternative to solving Chapman-Kolmogorov equations in terms of averages over individual realizations of the evolution of a system and we make extensive use of such simulations in this paper. However, as noted above, the major drawback of KMC simulations is their inability to represent the consequences of competing rates in other than an algorithmic context.

The next step is to use a Kramers-Moyal-van Kampen expansion of the master equation [42] to extract a Fokker-Planck equation [45–47] that embodies the statistics of the height fluctuations of the original lattice model. The statistical equivalence of results produced by these two equations is demonstrated by comparing the morphological evolution obtained from the Langevin equation associated with the Fokker-Planck equation with that produced by KMC simulations. These comparisons are based on the surface roughness and lateral height correlations, so scaling exponents can be determined directly [29]. But we can also identify crossover regimes, and calculate other statistical properties of the morphology, such as amplitudes [48] and stationary roughness distributions [49].

Quite apart from providing a computational alternative to KMC simulations, the lattice Langevin equation offers a framework for examining the analytic properties of lattice growth models. This includes the relative importance of different types of noise (e.g. due to deposition, diffusion, and evaporation) in different growth regimes, and the behavior under coarse-graining transformations, either for the direct passage to the continuum limit [50, 51], or for generating initial conditions for renormalization-group trajectories. The latter is a key element for explaining the unexpected behavior of the Wolf-Villain [24, 26] and Edwards-Wilkinson [27, 28] models in higher spatial dimensions revealed by KMC simulations.

The organization of this paper is as follows. In Sec. II we formulate the Chapman-Kolmogorov and master equations for fluctuating surfaces. The Kramers-Moyal-van Kampen expansion of the master equation is carried out in Sec. III and includes a discussion of the analytic requirements of this expansion. The analysis of the equivalent Langevin equation [29] is the subject of Sec. IV. To simplify the derivation of this equation, we confine our discussion to one-dimensional substrates, although this is not an inherent limitation of our procedure. Indeed, as noted above, there are several examples of intriguing behavior of lattice models in higher dimensions and our method is well placed to contribute to the debate. The replacement of discrete by continuous height units necessitated by the Kramers-Moyal-van Kampen expansion has subtle consequences for the regularization of the threshold functions used to characterize local height environments in the transition rules. This is discussed in Appendix A.

The application of our method to the Edwards-Wilkinson and Wolf-Villain models is described in Secs. V and VI, where direct comparisons between the KMC and Langevin solutions are made for the roughness and the lateral height correlations. The Edwards-Wilkinson model is used to demonstrate the convergence of the Langevin to the KMC solution for these quantities as the "largeness" parameter in the Kramers-Moyal-van Kampen expansion is increased. For the Wolf-Villain model, our method reproduces the complex crossover sequence observed with KMC simulations [24] even without a converged solution. In Sec. VII, we apply our method to a model with random deposition and surface diffusion. The surface roughness calculated from the Langevin equation again reproduces the main statistical characteristics of the KMC simulations, including the temperature dependence of the initial crossover from random deposition. We discuss the wider implications of these results in Sec. VIII, including the existence of a continuum expression of lattice Langevin equations and the extension of our method to other types of lattice model and to heteroepitaxial systems. A summary of our main results is provided in Sec. IX.

Some of the results described here have appeared previously in brief communications [29, 50]. The purpose of this paper is to present a detailed derivation of our methodology and to demonstrate its capability for a range of models used to study the statistical properties of growing surfaces. Our derivation clarifies and extends the earlier discussion [17] of equations of motion for models of epitaxial growth and provides a rigorous connection between the variables used in KMC simulations and those that appear in Langevin equations.

II. THE MASTER EQUATION

We consider a one-dimensional lattice of length L on each site i of which ($1 \le i \le L$) is a column whose topmost particle is at height H_i. Every surface profile corresponds uniquely to an array $\mathbf{H} = \{H_1, H_2, \ldots, H_L\}$. The lattice constant and vertical spacing are both set to unity, so the lattice sites and column heights have integer values. Processes such as deposition, desorption, and surface diffusion (see below) cause the heights to change by integer increments at discrete times t_n. Since the transition rates of these processes depend only on the instantaneous surface profile, not on its history, the models we consider are all Markovian.

The central quantity for Markov processes is the transition probability

$$P(\mathbf{H}_n, t_n | \mathbf{H}_{n-1}, t_{n-1}) \equiv T_t(\mathbf{H}_n | \mathbf{H}_{n-1}) \,, \qquad (1)$$

where only the time difference $t = t_n - t_{n-1}$ enters on the right-hand side because of the homogeneity of the processes under consideration. The Chapman-Kolmogorov equation [42],

$$T_{t+t'}(\mathbf{H}_3|\mathbf{H}_1) = \sum_{\mathbf{H}_2} T_{t'}(\mathbf{H}_3|\mathbf{H}_2) T_t(\mathbf{H}_2|\mathbf{H}_1) \,, \qquad (2)$$

is an identity for the transition probability of all Markov processes, but is rarely [43] amenable to a direct analysis. The differential form of this equation, expressed in terms of the small-time limit of the transition probability, is the master equation:

$$\frac{\partial T_t(\mathbf{H}_3|\mathbf{H}_1)}{\partial t} = \sum_{\mathbf{H}_2} \big[W(\mathbf{H}_3|\mathbf{H}_2) T_t(\mathbf{H}_2|\mathbf{H}_1) - W(\mathbf{H}_2|\mathbf{H}_3) T_t(\mathbf{H}_3|\mathbf{H}_1) \big] \,, \qquad (3)$$

where $W(\mathbf{H}'|\mathbf{H})$, the transition rate per unit time from $\mathbf{H}$ to $\mathbf{H}'$, is the time derivative of $T_t(\mathbf{H}'|\mathbf{H})$ evaluated at $t = 0$. This equation can be cast into a more compact and intuitive form by noting that each transition probability is evaluated for the initial state $\mathbf{H}_1$ at time t_1. Thus, by suppressing the redundant arguments, we can define $P(\mathbf{H}, t) \equiv T_t(\mathbf{H}|\mathbf{H}_1)$ and write Eq. (3) as [42]

$$\frac{\partial P}{\partial t} = \sum_{\mathbf{r}} \big[W(\mathbf{H} - \mathbf{r}; \mathbf{r}) P(\mathbf{H} - \mathbf{r}, t) - W(\mathbf{H}; \mathbf{r}) P(\mathbf{H}, t) \big] \,, \qquad (4)$$

where $W(\mathbf{H}; \mathbf{r})$ is the transition rate from $\mathbf{H}$ to $\mathbf{H}+\mathbf{r}$, and $\mathbf{r} = \{r_1, r_2, \ldots\}$ is the array of jump lengths r_i associated with each site.

The Chapman-Kolmogorov equation (2) is the definitive statement of the morphological evolution of our driven surfaces. Solutions of this equation provide the same statistical information as averages obtained from KMC simulations. The master equation (4) is a formal restatement of the Chapman-Kolmogorov equation in terms of a continuous time variable, but with discrete height variables. To render this equation physically meaningful, we must establish the relationship between the original variables and those appearing in Eq. (4). This will be done in Sec. III.

The transition rates are determined by processes that cause the heights to change. Typical examples for surface growth are deposition, surface diffusion, and evaporation. Expressions for the transition rates of such processes are easily constructed. For deposition, particles impinge on the lattice at an average rate τ_0^{-1} per site, where τ_0 is the time for the deposition of a monolayer of atoms. The transition rate W is nonvanishing only between configurations $\mathbf{H}$ and $\mathbf{H}'$ that differ by one height unit at the deposition site: $H_i' = H_i + 1$ for any site i. In the simplest case, random deposition, particles are deposited onto randomly chosen sites and remain there. The transition rate for this process is

$$W_1(\mathbf{H}; \mathbf{r}) = \tau_0^{-1} \sum_i \delta_{r_i,1} \prod_{j \ne i} \delta(r_j) \,, \qquad (5)$$

where $\delta_{i,j}$ is the Kronecker delta. If the final deposition site is selected from among the initial randomly chosen site and the two nearest neighbor sites according to some criterion, the transition rate becomes

$$W_2(\mathbf{H}; \mathbf{r}) = \tau_0^{-1} \sum_i \Bigg[w_i^{(1)} \delta_{r_i,1} \prod_{j \ne 1} \delta(r_j) + w_i^{(2)} \delta_{r_{i-1},1} \prod_{j \ne i-1} \delta(r_j) + w_i^{(3)} \delta_{r_{i+1},1} \prod_{j \ne i+1} \delta(r_j) \Bigg] \,, \qquad (6)$$

where the quantities $w_i^{(k)}$ express the conditions for the particle to remain on the initial site i ($k = 1$), to relax to the site $i-1$ ($k = 2$), or to relax to $i+1$ ($k = 3$). The sum rule

$$w_i^{(1)} + w_i^{(2)} + w_i^{(3)} = 1 \qquad (7)$$

ensures that the average deposition rate per site is τ_0^{-1}. The generalization of these expressions to deposition rules that include more distant neighbors is straightforward.

The transition rate for a particle hopping from a site i to a site j has the general form

$$W_3(\mathbf{H}; r) = \sum_{ij} w_{ij} \delta_{r_i,-1} \delta_{r_j,1} \prod_{k \ne i,j} \delta(r_k) \,, \qquad (8)$$

where the hopping rate and hopping rules are contained in the w_{ij}. The rules can depend on the initial configuration only, as for many models of surface diffusion [17], or on both the initial and final configurations, as for hopping near step-edge barriers [52] and Metropolis implementations of hopping [53]. A common model for surface diffusion is nearest neighbor hopping with Arrhenius rates whose energy barrier E_i is calculated from the initial environment of the active atom. In this case we have

$$w_{ij} = \tfrac{1}{2} \nu_0 e^{-\beta E_i} \left(\delta_{i,j-1} + \delta_{i,j+1} \right) \,, \qquad (9)$$

where the attempt frequency $\nu_0 \sim 10^{12}$–10^{13} s^{-1} [54], $\beta = (k_B T)^{-1}$, k_B is Boltzmann's constant, and T is the absolute temperature of the substrate. The simplest expression for E_i is obtained as the sum of a site-independent energy barrier E_S from the substrate and a contribution E_N from each of the n_i lateral nearest neighbors: $E_i = E_S + n_i E_N$. For comparisons with the morphologies of specific materials systems, these barriers can be determined either by fits to a particular experiment [3, 40] or from first-principles calculations [41].

III. KRAMERS-MOYAL-VAN KAMPEN EXPANSION

Although the master equation (4) is more manageable than the Chapman-Kolmogorov equation (2), direct solutions for driven surfaces are possible in only a few special cases [44]. To circumvent this problem, we will use a Kramers-Moyal-van Kampen expansion [42] and invoke a limit theorem to obtain a Fokker-Planck equation that embodies the statistical properties of the master equation. The Fokker-Planck equation and its associated Langevin equation are formulated in terms of continuous time and height variables that can be directly related to the original discrete variables used in Eq. (2). This procedure necessitates expanding the first term on the right-hand side of Eq. (4), which relies on two criteria for the transition rates [42]. These are discussed in the following two subsections.

A. The "Small Jump" Criterion

The first condition mandates that $W(\mathbf{H};\mathbf{r})$ is a sharply-peaked function of $\mathbf{r}$ in that there is a quantity $\delta > 0$ such that

$$W(\mathbf{H};\mathbf{r}) \approx 0 \quad \text{for} \quad |\mathbf{r}| > \delta\,. \tag{10}$$

This restricts the magnitude of the changes in $\mathbf{H}$ caused by the transition rules and is accordingly referred to as a "small jump" condition. The fulfillment of this condition ensures the convergence of the moments of $W(\mathbf{H};\mathbf{r})$, as discussed in Sec. III C.

Transition rules of lattice growth models typically change the column heights H_i by a single unit, as in Eqs. (5), (6), and (8). For these processes, the jump lengths $r_i = -1, 0$ or 1 for all sites i, which manifestly satisfies Eq. (10). This condition remains valid even for ballistic deposition, where a height can change by several units during a single deposition event [4].

B. The "Smoothness" Criterion

The second condition is that $W(\mathbf{H};\mathbf{r})$ is a slowly-varying function of $\mathbf{H}$, i.e.

$$W(\mathbf{H}+\Delta\mathbf{H};\mathbf{r}) \approx W(\mathbf{H};\mathbf{r}) \quad \text{for} \quad |\Delta\mathbf{H}| < \delta\,. \tag{11}$$

In effect, this is a smoothness criterion that renders the Kramers-Moyal-van Kampen expansion meaningful [55].

Transition rules such as those in Eqs. (5), (6), and (8) are typically expressed in terms of nonanalytic threshold functions that characterize the local height environment. For example, the number n_i of lateral nearest neighbors at a site i is calculated by determining how many nearest neighbor heights are greater than or equal to H_i:

$$n_i = \theta(H_{i-1} - H_i) + \theta(H_{i+1} - H_i)\,, \tag{12}$$

where

$$\theta(x) = \begin{cases} 1 & \text{if } x \geq 0; \\ 0 & \text{if } x < 0. \end{cases} \tag{13}$$

Thus, an arbitrarily small change in a height can lead to an abrupt change in n_i and thereby in any transition rate that depends on this quantity, in clear violation of Eq. (11). This problem can be alleviated by making two formal modifications to the transition rules. The unit jumps in Eqs. (5), (6), and (8) are replaced by jumps of size Ω^{-1}, where Ω — the "largeness" parameter in the van Kampen expansion [42] — controls the magnitude of the intrinsic fluctuations of the growth front:

$$H_i \to h_i = \Omega^{-1} H_i\,. \tag{14}$$

The time is rescaled accordingly as

$$t \to \tau = \Omega^{-1} t \tag{15}$$

to preserve the rates of change of the heights. The second modification is the replacement of the step function $\theta(x)$ in Eq. (13) by a *continuous* function. This renders the transition rates continuous as well, but the specific form of this regularization depends on the transition rules of the model under consideration. This is developed in Appendix A.

By regarding $\mathbf{h}$ and $\mathbf{r}$ as continuous variables, the master equation in (4) becomes

$$\frac{\partial P}{\partial \tau} = \int \left[\widetilde{W}(\mathbf{h}-\mathbf{r};\mathbf{r}) P(\mathbf{h}-\mathbf{r},\tau) - \widetilde{W}(\mathbf{h};\mathbf{r}) P(\mathbf{h},\tau) \right] d\mathbf{r}\,, \tag{16}$$

where the transformed transition rate $\widetilde{W}$ is, for example, given by

$$\widetilde{W}_1(\mathbf{h};\mathbf{r}) = \tau_0^{-1} \Omega \sum_i \delta\left(r_i - \frac{1}{\Omega}\right) \prod_{j \neq i} \delta(r_j)\,, \tag{17}$$

where $\delta(x)$ is the Dirac delta-function, with analogous expressions for $\widetilde{W}_2$ and $\widetilde{W}_3$ corresponding to Eqs. (6) and (8). Equation (16) describes the morphological evolution of the same model as the Chapman-Kolmogorov equation (2), but on time and heights scales that are finer by a factor Ω.

C. Fokker-Planck Equation

The first term on the right-hand side of Eq. (16) can now be expanded as a Taylor series to obtain

$$\int \widetilde{W}(\mathbf{h}-\mathbf{r};\mathbf{r})P(\mathbf{h}-\mathbf{r},\tau)\,d\mathbf{r} - \int \widetilde{W}(\mathbf{h};\mathbf{r})P(\mathbf{h},\tau)\,d\mathbf{r} = \sum_{n=1}^{\infty}\frac{(-1)^n}{n!}\sum_{i_1,\ldots,i_n}\frac{\partial^n}{\partial h_{i_1}\cdots\partial h_{i_n}}\left[K^{(n)}_{i_1\cdots i_n}(\mathbf{h})P(\mathbf{h},t)\right], \tag{18}$$

where $K^{(n)}_{i_1\cdots i_n}$ is the nth moment of $\widetilde{W}$,

$$K^{(n)}_{i_1\cdots i_n}(\mathbf{h}) = \int r_{i_1}\cdots r_{i_n}\widetilde{W}(\mathbf{h};\mathbf{r})\,d\mathbf{r} \sim O(\Omega^{1-n}). \tag{19}$$

The small jump condition in Eq. (10) ensures that these moments are well-defined. With this ordering in Ω of the $K^{(n)}$, a limit theorem due to Kurtz [45–47] states that, as $\Omega\to\infty$, the solution of the master equation (4) is approximated, with an error of $O(\ln\Omega/\Omega)$, by the solution of the Fokker-Planck equation [56],

$$\frac{\partial P(\mathbf{h},\tau)}{\partial\tau} = -\sum_i\frac{\partial}{\partial h_i}\left[K^{(1)\infty}_i(\mathbf{h})P(\mathbf{h},\tau)\right] + \frac{1}{2}\sum_{ij}\frac{\partial^2}{\partial h_i\partial h_j}\left[K^{(2)\infty}_{ij}(\mathbf{h})P(\mathbf{h},\tau)\right], \tag{20}$$

where, from Eq. (19), the first two moments of $\widetilde{W}$ are

$$K^{(1)\infty}_i(\mathbf{h}) \equiv \int r_i W(\mathbf{h};\mathbf{r})\,d\mathbf{r}, \tag{21}$$

$$K^{(2)\infty}_{ij}(\mathbf{h}) \equiv \int r_i r_j W(\mathbf{h};\mathbf{r})\,d\mathbf{r}. \tag{22}$$

This Fokker-Planck equation is expressed in terms of the continuous variables τ and $\mathbf{h}$ and provides the same statistical information about the morphological evolution of fluctuating surfaces as the Chapman-Kolmogorov equation (2), which is expressed in terms of the original discrete variables t and $\mathbf{H}$. These variables have a direct correspondence over their entire ranges only for $\Omega\to\infty$. This fact is signified by the superscript "∞" in the moments of the transition rate. The important conceptual and practical point is that the continuous representation is characterized completely by a deterministic drift $K^{(1)\infty}_i$ and diffusion with coefficients $K^{(2)\infty}_{ij}$.

IV. THE LANGEVIN EQUATION

The solution of Eq. (20) will be obtained by solving the equivalent Langevin equation [42, 47],

$$\frac{dh_i}{d\tau} = K^{(1)\infty}_i(\mathbf{h}) + \eta_i, \tag{23}$$

where the η_i are Gaussian noises with mean zero and a covariance matrix given by $K^{(2)\infty}$:

$$\langle\eta_i(\tau)\rangle = 0, \tag{24}$$

$$\langle\eta_i(\tau)\eta_j(\tau')\rangle = K^{(2)\infty}_{ij}(\mathbf{h})\delta(\tau-\tau'), \tag{25}$$

and $\langle\cdot\rangle$ signifies averages with respect to the distribution function of the η_i. The initial and boundary conditions for this coupled set of differential equations must be the same as those used for obtaining KMC solutions of the Chapman-Kolmogorov equation (2). The initial condition is given by a configuration $\mathbf{h}_0 = \{h_1(0), h_2(0), \ldots, h_L(0)\}$. Periodic boundary conditions are used in all the calculations reported here.

The solution of the Langevin equation (23) produces results that are statistically equivalent to the Chapman-Kolmogorov equation in that averages over many independent realizations are identical. This relationship can be expressed formally as

$$\big\langle F\big(\{H_i(t)\}\big)\big\rangle = \Big\langle F\Big(\big\{H_i(0) + \textstyle\int_0^t\left[K^{(1)\infty}_i(\mathbf{h}(\tau)) + \eta_i(\tau)\right]d\tau\big\}\Big)\Big\rangle, \tag{26}$$

where F is a function of the surface profile, such as the width or the structure factor defined in Sec. IV B. This equation provides a direct connection between the continuous variables τ and h_i in the Langevin equation and the discrete variables t and H_i used for KMC solutions of the Chapman-Kolmogorov equation.

For models of deposition and instantaneous relaxation, as in Eq. (6), each event changes the occupancy only of a single site. Thus, all of the moments of W are diagonal and proportional to the first moment, and we have

$$K^{(1)\infty}_i = \frac{1}{\tau_0}\left[w^{(1)}_i + w^{(2)}_{i+1} + w^{(3)}_{i-1}\right], \tag{27}$$

$$K^{(2)\infty}_{ij} = \delta_{ij}K^{(1)\infty}_i, \tag{28}$$

so the noise covariance in Eq. (25) reduces to

$$\langle\eta_i(\tau)\eta_j(\tau')\rangle = K^{(1)\infty}_i\delta_{ij}\delta(\tau-\tau'). \tag{29}$$

Alternatively, for models with random deposition and concurrent surface diffusion described by the nearest neighbor hopping in Eq. (9) the transition moments are

$$K^{(1)\infty}_i = \tfrac{1}{2}\nu_0\Delta^2\lambda_i + \tau_0^{-1}, \tag{30}$$

$$K^{(2)\infty}_{ij} = \tfrac{1}{2}\nu_0\left[\delta_{ij}\Delta^2\lambda_i - (\lambda_i+\lambda_j)\Delta^2\delta_{ij}\right] + \tau_0^{-1}\delta_{ij}, \tag{31}$$

where $\lambda_i = e^{-\beta E_i}$, and the discrete second difference

$$\Delta^2 f_i = f_{i-1} - 2f_i + f_{i+1} \tag{32}$$

acts only on the first index of δ_{ij} in Eq. (31). Any hopping process generates off-diagonal matrix elements in the covariance matrix because the occupancies of two sites are changed by such an event. Nearest neighbor hopping produces a tridiagonal covariance matrix, while longer range hopping and cluster diffusion generate associated non-zero entries in this matrix.

A. Numerical Solution of the Langevin Equation

The numerical integration of Eqs. (23) and (25) proceeds by assigning an Itô interpretation to the noise [47]. We first consider deposition models. The stochastic differential equation associated with the Langevin equation (23) and the moments in Eqs. (27) and (28) is

$$dh_i = K_i^{(1)\infty}(\mathbf{h})\, d\tau + \left[K_i^{(1)\infty}(\mathbf{h})\right]^{1/2} dW_i\,, \qquad (33)$$

where the Wiener variable dW_i represents continuous Brownian motion [57]. The square root of the diagonal matrix $K^{(1)\infty}$ is well-defined because all of the matrix elements in Eq. (28) are non-negative. This equation is discretized as

$$h_i(\tau+\Delta\tau) = h_i(\tau) + K_i^{(1)\infty}(\mathbf{h})\,\Delta\tau + \left[K_i^{(1)\infty}(\mathbf{h})\right]^{1/2}\Delta W_i(\tau)\,, \qquad (34)$$

with $\Delta W_i(\tau) = W_i(\tau+\Delta\tau) - W_i(\tau)$, and

$$\langle \Delta W_i(\tau)\rangle = 0\,, \qquad (35)$$

$$\langle [\Delta W_i(\tau)]^2\rangle = \Delta\tau\,. \qquad (36)$$

The diagonal covariance matrix for deposition models considerably simplifies the numerical integration of Eq. (23) because different sites are coupled only in the computation of the diagonal elements. For models with surface diffusion, however, the covariance matrices have non-zero off-diagonal entries, as in Eq. (31), so an altogether different scenario arises. The formulation of the corresponding stochastic differential equation relies on the fact that this matrix is positive definite, i.e.

$$\sum_{i,j=1}^{L} K_{ij}^{(2)\infty} v_i v_j > 0\,, \qquad (37)$$

for all nonzero vectors $\mathbf{v} = (v_1, \ldots, v_L)$. For the matrix elements in Eq. (31), we calculate

$$\sum_{i,j=1}^{L} K_{ij}^{(2)\infty} v_i v_j = \sum_{i=1}^{L} (\lambda_{i-1}+\lambda_i)(v_{i-1}-v_i)^2 + \frac{v^2}{\tau_0}\,, \qquad (38)$$

where periodic conditions have been imposed on the matrix elements and on the components of $\mathbf{v}$. Thus, for any finite deposition rate, $K^{(2)\infty}$ is positive definite. For equilibration in the absence of deposition (Sec. VII), we must therefore impose an arbitrarily small flux to maintain this property.

Given the foregoing, the stochastic differential equation associated with the Langevin equation (23) and the moments in Eqs. (30) and (31) can be written as

$$dh_i = K_i^{(1)\infty}(\mathbf{h})\, d\tau + \sum_{j=1}^{L} U_{ij}\, dW_j\,, \qquad (39)$$

in which $U^{\mathrm{T}}U = K^{(2)\infty}$, where U^{T} is the transpose of U, is the Cholesky factorization [58] of the symmetric positive definite matrix $K^{(2)\infty}$ in terms of the upper triangular matrix U. The discretized form of this equation is given by

$$h_i(\tau+\Delta\tau) = h_i(\tau) + K_i^{(1)\infty}\,\Delta\tau + \sum_{j=1}^{L} U_{ij}\Delta W_j(\tau)\,, \qquad (40)$$

where

$$\langle \Delta W_i(\tau)\rangle = 0\,, \qquad (41)$$

$$\langle \Delta W_i(\tau)\Delta W_j(\tau)\rangle = \delta_{ij}\Delta\tau\,. \qquad (42)$$

The Cholesky decomposition required for the integration of Eq. (40) can place substantial demands on computer resources for large system sizes if extended deposition times are required.

The results presented in the following sections are obtained by integrating Eqs. (34) and (40) for decreasing values of $\Delta\tau$. According to Eqs. (14) and (15), $h_i = \Omega^{-1}H_i$ and $\tau = \Omega^{-1}t$, so $\Delta h_i = \Omega^{-1}\Delta H_i$ and $\tau = \Omega^{-1}\Delta t$, which implies that a decrease in $\Delta\tau$ is equivalent to an increase of Ω. Hence, with increasing Ω successively more iterations of Eqs. (34) and (40) are required to reach the same elapsed real time interval Δt and physical height change ΔH_i. Since all our models are subsumed by the general equation (40), we write the discretized form of Eq. (26) as

$$\langle F(\{H_i(t)\})\rangle = \left\langle F\left(\left\{H_i(0) + \sum_{n=1}^{\Omega}\left[(\Omega^{-1}t)K_i^{(1)\infty}(\mathbf{h}(\tau_n)) + \sum_{j=1}^{L} U_{ij}\Delta W_j(\tau_n)\right]\right\}\right)\right\rangle, \qquad (43)$$

where $\tau_n = \Omega^{-1}nt$. The evaluation of this equation proceeds by determining $K^{(1)\infty}$ and $K^{(2)\infty}$ from $\mathbf{h}(\tau_n)$. Gaussian random numbers with zero mean and unit variance are then used to determine the fluctuations at all lattice sites to obtain the height profile $\mathbf{h}(\tau_{n+1})$ at the next time step. As $\Omega \to \infty$, Kurtz's theorem [45–47] stipulates that the statistical properties of the morphology determined by averages of these solutions converge

to the corresponding average quantities obtained from KMC simulations.

B. Statistical Characterization of Rough Surfaces

Our comparisons between KMC simulations and solutions of Langevin equations are based on the surface roughness and the lateral height correlation function. These quantities provide statistical information about the morphological evolution normal to and along the surface.

The surface roughness $W(L,t)$ is defined as the root-mean square of the height profile,

$$W(L,t) \equiv \left[\langle h^2(t)\rangle - \langle h(t)\rangle^2\right]^{1/2} , \tag{44}$$

where $\langle h(t)^n\rangle = L^{-1}\sum_i h_i^n(t)$ for $n = 1, 2$. For sufficiently long times and large substrate sizes, W exhibits dynamic scaling [4]:

$$W(L,t) \sim L^{\alpha} f(t/L^z) , \tag{45}$$

with the scaling function

$$f(x) \sim \begin{cases} x^{\beta} & \text{for } x \ll 1; \\ \text{constant} & \text{for } x \gg 1, \end{cases} \tag{46}$$

in which α is the roughness exponent, $z = \alpha/\beta$ is the dynamic exponent, and β is the growth exponent.

The lateral height correlation function $C(r,t)$ is defined as

$$C(r,t) \equiv \langle [h_i(t) - h_j(t)]^2\rangle^{1/2} , \tag{47}$$

where $r = |i-j|$ is the separation of sites i and j. For r much smaller than the lateral correlation length, C has the scaling form [4]

$$C(r,t) \sim r^{\alpha} . \tag{48}$$

The exponents α, β, and z provide the basis for assigning a model to a particular universality class and thereby inferring the associated continuum equation, in analogy with the procedure used for critical dynamics.

V. THE EDWARDS-WILKINSON MODEL

The Edwards-Wilkinson equation [30],

$$\frac{\partial h}{\partial t} = \nu_2 \frac{\partial^2 h}{\partial x^2} + \xi , \tag{49}$$

where $\nu_2 > 0$ and ξ is a Gaussian white noise, was originally proposed as a theory for sedimentation. The atomistic realizations of this model for surfaces driven by deposition from a molecular beam [20, 27, 28] are based on identifying the lowest height(s) near a randomly chosen site. In the version we study here, a particle incident on a site remains there only if its height is less than or equal to that of both of its nearest neighbors. If only one nearest neighbor column is lower than that of the original site, deposition is onto that site, but if both nearest neighbor heights are less than that of the original site, the deposition site is chosen randomly between the two lower columns.

The pertinent height configurations can be tabulated by using the step function in Eq. (13) to express the relative heights between the nearest neighbors of the initial site as an identity:

$$\begin{aligned} &[\theta(h_{i-1} - h_i) + \Theta(h_{i-1} - h_i)] \\ &\times [\theta(h_{i+1} - h_i) + \Theta(h_{i+1} - h_i)] = 1 , \end{aligned} \tag{50}$$

where

$$\Theta(h_i - h_j) = 1 - \theta(h_i - h_j) . \tag{51}$$

The expansion of Eq. (50) produces 4 configurations each of which is assigned to the $w_i^{(k)}$ in Eq. (6) according to the rules of the Edwards-Wilkinson model. The sum rule in Eq. (7) is thereby satisfied by construction. These assignments are shown in Fig. 1 and yield the expressions

$$w_i^{(1)} = \theta(h_{i-1} - h_i)\theta(h_{i+1} - h_i) , \tag{52}$$

$$\begin{aligned} w_i^{(2)} &= \theta(h_{i+1} - h_i)\Theta(h_{i-1} - h_i) \\ &\quad + \tfrac{1}{2}\Theta(h_{i-1} - h_i)\Theta(h_{i+1} - h_i) , \end{aligned} \tag{53}$$

$$\begin{aligned} w_i^{(3)} &= \theta(h_{i-1} - h_i)\Theta(h_{i+1} - h_i) \\ &\quad + \tfrac{1}{2}\Theta(h_{i-1} - h_i)\Theta(h_{i+1} - h_i) . \end{aligned} \tag{54}$$

The Langevin equation for the Edwards-Wilkinson model is obtained by substituting these expressions into Eqs. (23) and (25).

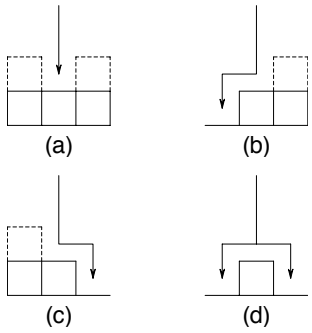

FIG. 1: Relaxation rules of the Edwards-Wilkinson model, with contributions to (a) $w_i^{(1)}$, (b) $w_i^{(2)}$, (c) $w_i^{(3)}$, and (d) to $w_i^{(2)}$ and $w_i^{(3)}$. The corresponding expressions are given in Eqs. (52)–(54). The arrows indicate the incident and deposition sites. In (d), both of the deposition sites are equally likely. The broken lines show where greater heights do not affect the deposition site.

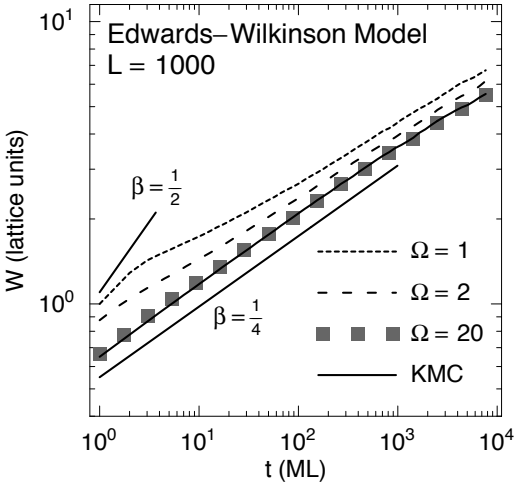

FIG. 2: Surface roughness obtained from the Langevin equation (23) and (25) with Eqs. (52)-(54) and from KMC simulations for a system of length $L = 1000$ for $\Omega = 1, 2, 20$. Time is measured in units of monolayers (ML) deposited. The data were averaged over 500 independent realizations. The slopes of the straight lines correspond to the growth exponent of random deposition ($\beta = \frac{1}{2}$) and that of the Edwards-Wilkinson model ($\beta = \frac{1}{4}$).

The comparison of $W(L,t)$ obtained from KMC simulations and the Langevin equation employing the step function $\theta(x;0)$ in Eq. (A1) is shown in Fig. 2 for a system of length $L = 1000$ and with $\Omega = 1, 2, 20$. Most apparent is that, for $\Omega = 1, 2$, the roughness calculated from the Langevin equation is appreciably greater than that of the KMC simulation. For $\Omega = 1$ there is a spurious "crossover" near 2–3 ML from random deposition, characterized by a growth exponent $\beta = \frac{1}{2}$, toward the Edwards-Wilkinson scaling regime at times beyond $t \sim 10^2$ ML. The behavior at early times is due largely to the noise: the covariance matrix in Eq. (25) includes information about nearest-neighbor sites, but the noise is uncorrelated between sites. Thus, as the lattice is scanned at each time step, the uncorrelated noise produces a larger variance in the heights than that of the simulation. As Ω increases this regime collapses toward $t = 0$ and the roughness calculated from the Langevin equation converges to the KMC roughness at all times.

Figure 3 compares the lateral height correlation function in Eq. (47) obtained from KMC simulations for a lattice of size $L = 1000$ with that determined from the Langevin equation for $\Omega = 1, 2, 20$ at an early time ($t = 100$ ML) and at a much later time ($t = 5000$ ML). The basic trends with increasing Ω are the same as those in Fig. 2. The Langevin solution overestimates the correlation function and there is a crossover from uncorrelated behavior, characteristic of random deposition, to the Edwards-Wilkinson scaling regime. These deviations are most apparent up to $r \sim 10$, even for $\Omega = 20$. This is to be expected, since the spatial range of the discrepancy approaches the atomic scale of the lattice. However, even

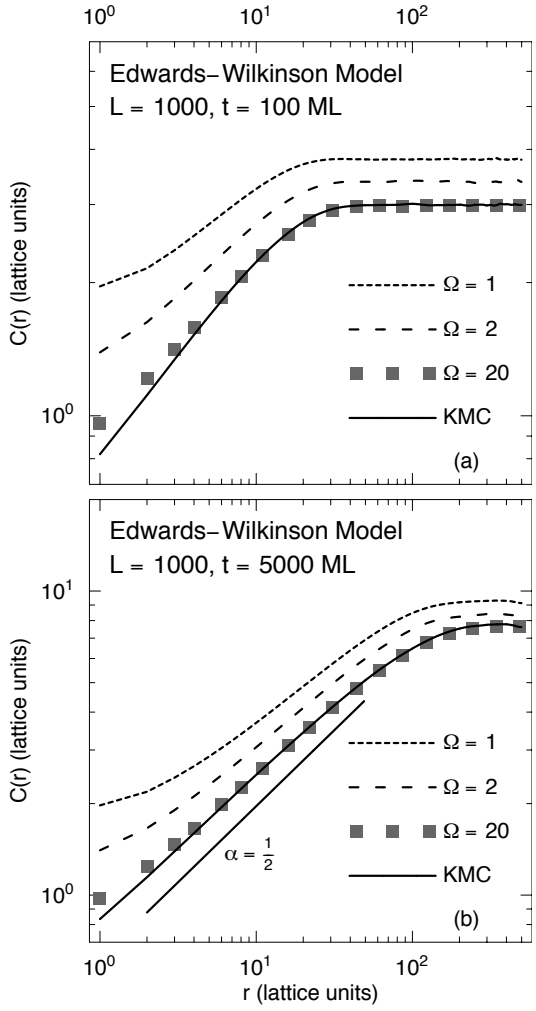

FIG. 3: Lateral height correlation function obtained from the Langevin equation (23) and (25) with Eqs. (52)-(54) and KMC simulations up to $r = 500$ for a system of size $L = 1000$ at (a) $t = 100$ ML and (b) $t = 5000$ ML for $\Omega = 1, 2, 20$. Data were obtained by averaging over 500 independent realizations. The slope of the straight line in (b) has the Edwards-Wilkinson value of the roughness exponent ($\alpha = \frac{1}{2}$).

for $\Omega = 1$ the spatial range of the correlations is correctly described by the Langevin equation.

We have shown previously [29] that a plot of $WL^{-\alpha}$ *vs.* tL^{-z} produces a collapse onto the scaling function f in Eq. (45) for the Edwards-Wilkinson exponents ($\alpha = \frac{1}{2}, z = 2$). This result, together with the comparisons in Figs. 2 and 3, shows that, for large enough values of Ω, our method reproduces the pre-asymptotic behavior, the scaling properties, and the saturation values of the roughness and correlation function obtained from KMC simulations. The roughness fluctuations in the saturation regime [49] also follow the same scaling function as the KMC solution [59]. Each of these quantities interrogates a different aspect of the surface morphology, so the comparisons presented in this section demonstrate that our method yields results that systematically converge

to those of KMC simulations as $\Omega \to \infty$. Indeed, these comparisons suggest that, if only the scaling regimes are of interest, then solutions of the Langevin equation, even with $\Omega = 1$ for large enough system sizes and long enough times, yield an accurate estimate of the exponents.

VI. THE WOLF-VILLAIN MODEL

The Wolf-Villain model [32] was first introduced for the low-temperature growth of group-IV materials [31]. This model has been the subject of many theoretical studies [18, 23, 24, 60–63, 65, 66]. KMC simulations show a slow crossover from Mullins-Herring to Villain-Lai-Das Sarma behavior and eventually to the Edwards-Wilkinson universality class [24, 62, 63], a conclusion supported by arguments based on surface diffusion currents [23].

In the Wolf-Villain model [31, 32] an arriving particle remains on the original (randomly chosen) site only if its coordination cannot be increased by moving to a nearest neighbor site. If only one nearest neighbor site offers greater coordination than the original site, deposition is onto that site. However, if both nearest neighbor sites offer greater coordination than the original site, the deposition site is chosen randomly between the two. The required configurations can be tabulated by using the step functions in Eqs. (13) and (51) to express the pertinent relative heights as an identity. Since the coordinations of the initial and two nearest neighbor sites are needed to ascertain the deposition site, this identity must include sites up to second-nearest neighbors:

$$\begin{aligned}
&[\theta(h_{i-1} - h_{i-2}) + \Theta(h_{i-1} - h_{i-2})] \\
&\times [\delta(h_i, h_{i-1}) + \Theta(h_{i-1} - h_i) + \Theta(h_i - h_{i-1})] \\
&\times [\delta(h_i, h_{i+1}) + \Theta(h_i - h_{i+1}) + \Theta(h_{i+1} - h_i)] \\
&\times [\theta(h_{i+1} - h_{i+2}) + \Theta(h_{i+1} - h_{i+2})] = 1\,, \qquad (55)
\end{aligned}$$

where

$$\delta(h_i, h_j) = \theta(h_i - h_j) + \theta(h_j - h_i) - 1\,. \qquad (56)$$

The expansion of Eq. (55) produces 36 terms that can be combined into distinct generic configurations and assigned to the $w_i^{(j)}$ according to the deposition rules of the Wolf-Villain model. The deposition rules are depicted in Fig. 4 for $w_i^{(1)}$ and in Fig. 5 for $w_i^{(2)}$. The associated diagrams for $w_i^{(3)}$ are mirror images about the central (ith) site of each diagram in Fig. 5. Expressions for the configurations in Figs. 4 and 5 are compiled in Table I; the corresponding expressions for the configurations that contribute to $w_i^{(3)}$ can be obtained by applying the transformation $i \pm k \to i \mp k$ to each of the terms for $w_i^{(2)}$. We mention in passing that the corresponding constructions in Table I and Figs. 4 and 5 for the Das Sarma-Tamborenea model [33] requires minimal additional effort because the generic configurations are the same as those of the Wolf-Villain model. The two models differ only in the implementation of their deposition rules to these configurations.

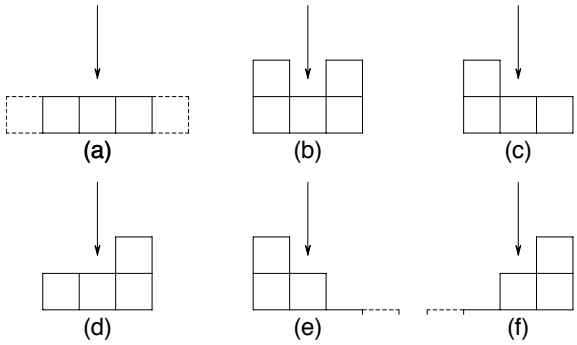

FIG. 4: Local height configurations that contribute to $w_i^{(1)}$ for the Wolf-Villain model. Arrows indicate the incident and deposition sites. Column heights strictly greater than and strictly equal to h_i are as indicated; those less than or equal to h_i are shown with broken lines.

Figure 6 compares the roughness determined from KMC simulations with that obtained from the Langevin equation with the step function $\theta(x;1)$ in Eq. (A1) for a lattice of length $L = 40\,000$. Because of the extended deposition time and large system size, we have integrated the Langevin equation with $\Omega = 1$. In common with the corresponding comparison for the Edwards-Wilkinson model in Fig. 2, there is an initial transient regime extending up to $t \sim 10$ ML during which $\beta \simeq 0.5$, corresponding to random deposition. For greater times, the roughness obtained from the Langevin equation tracks the KMC roughness.

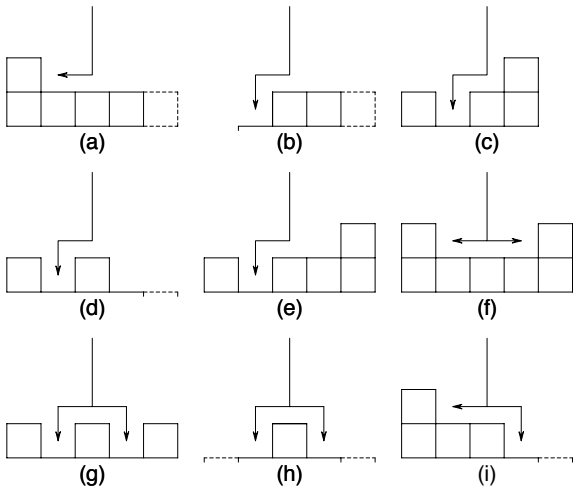

FIG. 5: Local height configurations that contribute to $w_i^{(2)}$ for the Wolf-Villain model. Arrows indicate the incident and deposition sites. Where more than one deposition site is obtained, both are equally likely. Column heights strictly greater than and strictly equal to h_i are as indicated: those less than or equal to h_i are shown with broken lines.

TABLE I: The terms generated by the expansion of Eq. (55), the corresponding configurations in Figs. 4 and 5, and the assignment to the $w_i^{(j)}$ according to the rules of the Wolf-Villain model.

Term	Figure	Rule
$\theta(h_{i-1}-h_{i-2})\delta(h_i,h_{i-1})\delta(h_i,h_{i+1})\theta(h_{i+1}-h_{i+2})$	4(a)	$w_i^{(1)}$
$\big[1-\theta(h_i-h_{i-1})\big]\big[1-\theta(h_i-h_{i+1})\big]$	4(b)	$w_i^{(1)}$
$\big[1-\theta(h_i-h_{i-1})\big]\delta(h_i,h_{i+1})$	4(c)	$w_i^{(1)}$
$\delta(h_i,h_{i-1})\big[1-\theta(h_i-h_{i+1})\big]$	4(d)	$w_i^{(1)}$
$\big[1-\theta(h_i-h_{i-1})\big]\big[1-\theta(h_{i+1}-h_i)\big]\theta(h_{i+1}-h_{i+2})$	4(e)	$w_i^{(1)}$
$\theta(h_{k-1}-h_{k-2})\big[1-\theta(h_{i-1}-h_i)\big]\big[1-\theta(h_i-h_{i+1})\big]$	4(f)	$w_i^{(1)}$
$\big[1-\theta(h_{i-1}-h_{i-2})\big]\delta(h_i,h_{i-1})\delta(h_i,h_{i+1})\theta(h_{i+1}-h_{i+2})$	5(a)	$w_i^{(2)}$
$\big[1-\theta(h_{i-1}-h_i)\big]\delta(h_i,h_{i+1})\theta(h_{i+1}-h_{i+2})$	5(b)	$w_i^{(2)}$
$\big[1-\theta(h_{i-1}-h_{i-2})\big]\big[1-\theta(h_{i-1}-h_i)\big]\big[1-\theta(h_i-h_{i+1})\big]$	5(c)	$w_i^{(2)}$
$\big[1-\theta(h_{i-1}-h_{i-2})\big]\big[1-\theta(h_{i-1}-h_i)\big]\big[1-\theta(h_{i+1}-h_i)\big]\theta(h_{i+1}-h_{i+2})$	5(d)	$w_i^{(2)}$
$\big[1-\theta(h_{i-1}-h_{i-2})\big]\big[1-\theta(h_{i-1}-h_i)\big]\delta(h_i,h_{i+1})\big[1-\theta(h_{i+1}-h_{i+2})\big]$	5(e)	$w_i^{(2)}$
$\big[1-\theta(h_{i-1}-h_{i-2})\big]\delta(h_i,h_{i-1})\delta(h_i,h_{i+1})\big[1-\theta(h_{i+1}-h_{i+2})\big]$	5(f)	$w_i^{(2)}, w_i^{(3)}$
$\big[1-\theta(h_{i-1}-h_{i-2})\big]\big[1-\theta(h_{i-1}-h_i)\big]\big[1-\theta(h_{i+1}-h_i)\big]\big[1-\theta(h_{i+1}-h_{i+2})\big]$	5(g)	$w_i^{(2)}, w_i^{(3)}$
$\theta(h_{i-1}-h_{i-2})\big[1-\theta(h_{i-1}-h_i)\big]\big[1-\theta(h_{i+1}-h_i)\big]\theta(h_{i+1}-h_{i+2})$	5(h)	$w_i^{(2)}, w_i^{(3)}$
$\big[1-\theta(h_{i-1}-h_{i-2})\big]\delta(h_i,h_{i-1})\big[1-\theta(h_{i+1}-h_i)\big]\theta(h_{i+1}-h_{i+2})$	5(i)	$w_i^{(2)}, w_i^{(3)}$

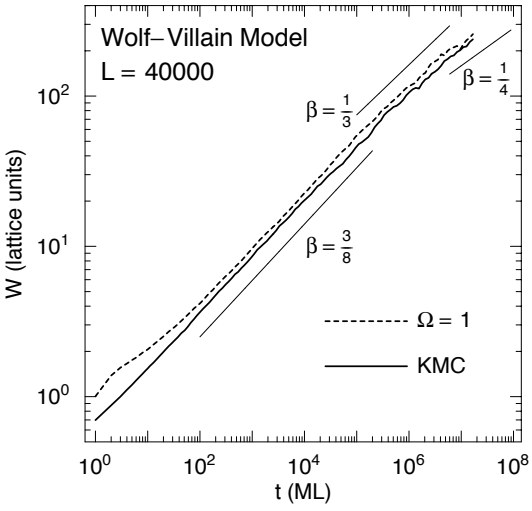

FIG. 6: Comparison of surface roughness obtained from the lattice Langevin equation with $\Omega = 1$ and KMC simulations for the Wolf-Villain model for a system of length $L = 40\,000$. Scaling regimes are shown by straight lines whose slopes have the indicated values of the growth exponent β.

After the initial transient period, for times up to 10^5 ML, the growth exponent is $\beta = \frac{3}{8}$, which corresponds to that of the Mullins-Herring equation [67, 68],

$$\frac{\partial h}{\partial t} = -\nu_4 \frac{\partial^4 h}{\partial x^4} + \xi\,, \tag{57}$$

where $\nu_4 > 0$. This is the result obtained by Wolf and Villain [32] from KMC simulations, but we can offer an analytic justification of this behavior. If, in the lattice Langevin equation, the step function $\theta(x;1)$ in Eq. (A1) and the height profile $\mathbf{h}$ are replaced by analytic functions, and discrete differences are calculated with Taylor expansions, the dominant coefficient, by almost an order of magnitude, in the resulting infinite series of partial derivatives is ν_4 [51]. Thus, the morphological evolution of the smoothed Wolf-Villain model is described approximately by the Mullins-Herring equation.

Mullins-Herring scaling persists for almost four decades of deposition time before crossing over to a regime characterized by the growth exponent $\beta = \frac{1}{3}$, which corresponds to the Villain-Lai-Das Sarma equation [9, 10]:

$$\frac{\partial h}{\partial t} = -\nu_4 \frac{\partial^4 h}{\partial x^4} + \lambda \frac{\partial^2}{\partial x^2}\left(\frac{\partial h}{\partial x}\right)^2 + \xi\,. \tag{58}$$

After a further elapsed time extending to two decades, there is a final crossover to the scaling regime of the Edwards-Wilkinson equation (49), for which $\beta = \frac{1}{4}$. Although the Langevin equation provides an accurate account of this crossover sequence, which was first reported by Kotrla and Šmilauer [24], a fundamental understanding requires an analysis of the renormalization-group trajectory from the initial conditions of the smoothed Wolf-Villain model. This will be reported elsewhere.

The correlation function in Eq. (47) determined from KMC simulations and the Langevin equation with $\Omega = 1$ is shown in Fig. 7 at times $t = 10^4$ ML, 10^6 ML, 10^8 ML. The comparison in Fig. 7(a) shows that the scaling

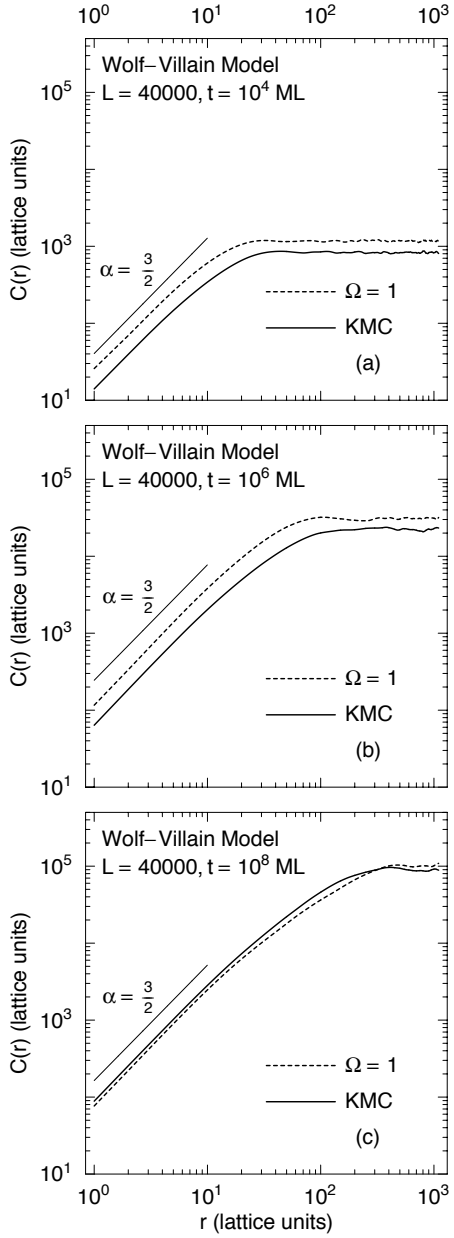

FIG. 7: The correlation function $C(r)$ defined in Eq. (47) calculated from KMC simulations and the Langevin equation with $\Omega = 1$ for the Wolf-Villain model for a system size of $L = 40\,000$ at times (a) 10^4 ML, (b) 10^6 ML, and (c) 10^8 ML.

regime of the correlation function is consistent with the roughness exponent $\alpha = \frac{3}{2}$ associated with the Mullins-Herring equation. This behavior persists to $t = 10^8$ ML [Fig. 7(b,c)], but only for values of r up to 10 lattice units, i.e. only for short-range correlations. At $t = 10^8$ ML, there appears to be an incipient crossover from the Mullins-Herring regime, but no other clearly discernible scaling regime. Nevertheless, the correlation function obtained from the Langevin solution follows the details of the KMC solution; any discrepancy can be attributed to our having used $\Omega = 1$ to obtain this solution. Even at the latest time, the correlations extend only to several hundred lattice sites, so the slope change in the roughness at this time is a true crossover, rather than the onset of saturation. In contrast, for the system in Figs. 2 and 3, the lateral correlations are approaching the system size and the roughness shows the first signs of saturation.

VII. RANDOM DEPOSITION WITH SURFACE DIFFUSION

Models of epitaxial kinetics typically include random deposition and nearest-neighbor Arrhenius-type hopping over barriers determined by the initial environment of the hopping atom [1–3]. As noted in Sec. IV, the simplest such rules stipulate that the hopping barrier is determined by an energy E_S from the substrate and a contribution E_N from each of the n_i lateral nearest neighbors, so $E_i = E_S + n_i E_N$. The Langevin equation for this model is given in terms of the moments in Eqs. (30) and (31) in which we take [3] $E_S = 1.58$ eV and $E_N = 0.24$ eV for a system of length $L = 100$. The deposition rate is 0.5 ML per second. We have used the step function $\theta(x;1)$ in Eq. (A1), which is the same as that used for the Wolf-Villain model because the transition rules are again determined by calculating the number of nearest neighbors.

The scaling behavior of this model has been studied with the renormalization-group [10] and KMC simulations [22, 70]. The roughness shows an intermediate scaling regime with a growth exponent $\beta = \frac{3}{8}$, characteristic of the Mullins-Herring equation (57), before crossing over to the value $\beta = \frac{1}{3}$ calculated [10] for the equation of motion in Eq. (58). Since these regimes are manifestations of thermally activated hopping, the crossover times decreases with increasing temperature.

Figure 8 compares the surface roughness in Eq. (44) determined by KMC simulations with that obtained from the solution of the Langevin equation for temperatures $T = 500$ K and $T = 600$ K. At $T = 500$ K [Fig. 8(a)], surface diffusion is almost completely suppressed and growth proceeds essentially by random deposition, resulting in the growth exponent $\beta = \frac{1}{2}$ characteristic of this process. In this regime, $\gamma \approx 1$ for all lattice sites, so the off-diagonal elements in the correlation matrix Eq. (31) are small compared to the diagonal elements, but we have retained all of the correlation matrix elements in this calculation. The weak surface diffusion means that the local environment is of minimal importance for the transition rules, so calculations with $\Omega = 1$ yield accurate results. However, surface diffusion is not completely absent, as times beyond 10^4 ML see the onset of the crossover to the Mullins-Herring growth exponent ($\beta = \frac{3}{8}$).

As the temperature is raised to 600 K, surface diffusion becomes activated and the roughness shows an altogether different behavior from that at 500 K [Fig. 8(b)]. After an initial transient, the growth exponent initially approaches $\beta = \frac{3}{8}$. The importance of surface diffusion

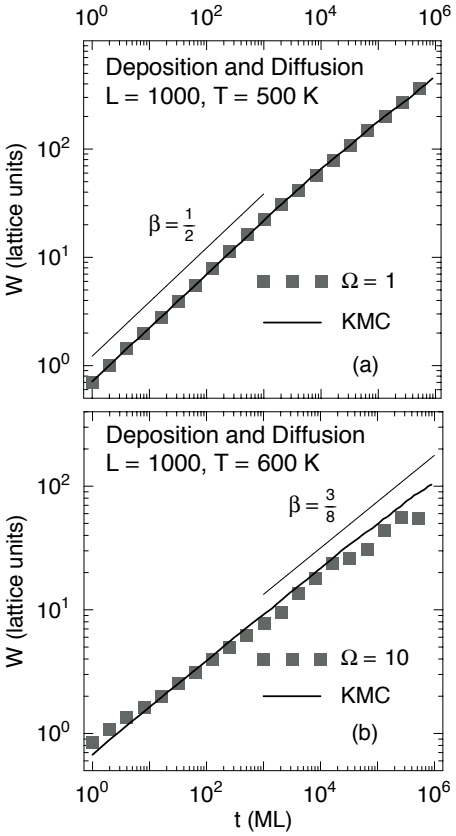

FIG. 8: Comparison between surface roughness obtained from the lattice Langevin equation with the indicated values of Ω and KMC simulations for a model with random deposition and surface diffusion for a system of length $L = 100$. The results have been averaged over 500 independent realizations.

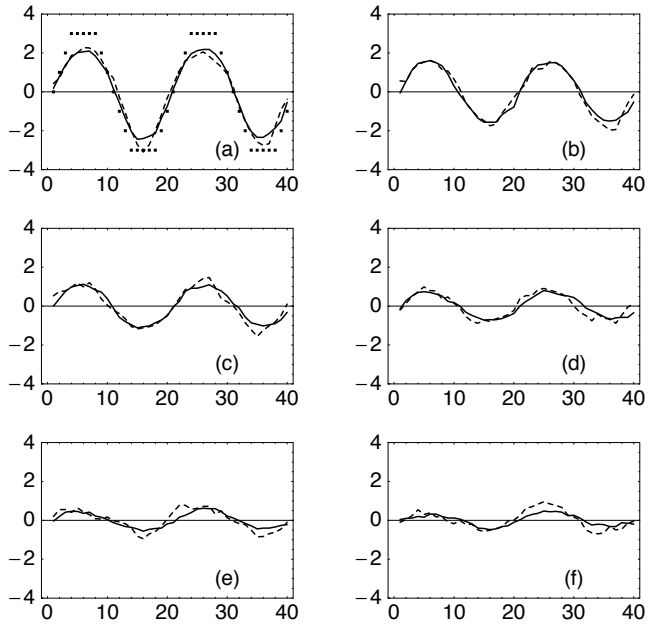

FIG. 9: Relaxation of a surface profile in the absence of deposition at 600 K modelled by KMC simulations (solid lines) and the Langevin equation with $\Omega = 20$ (broken lines). The system has size $L = 40$ on which periodic boundary conditions are imposed. The initial profile is indicated by dots in (a). Profiles are shown at times (a) 3000, (b) 6000, (c) 9000, (d) 12000, (e) 15000, and (f) 18000. In each panel, the abscissa is the spatial position ($1 \leq i \leq 40$) and the ordinate is the height h_i. The energy parameters are the same as those used in Fig. 8 and each result has been averaged over 50 independent realizations.

means that the local environment becomes an important factor in the transitions at this temperature, so a value of $\Omega = 10$ is required to obtain agreement between the Langevin and KMC solutions. These comparisons indicate that the Langevin equation captures the interplay between the driving force of the deposition process and the equilibration through surface diffusion, which is one of the central features of epitaxial growth.

The effect of surface diffusion can be isolated by examining the equilibration of a surface profile in the absence of deposition. Such studies originated with the work of Mullins [68] who showed that the relaxation of a sinusoidally patterned surface could be used to extract surface diffusion constants. Figure 9 shows a sequence of snapshots of the relaxation of the one-dimensional profile displayed in panel (a) determined by KMC simulations and from the solution of the Langevin equation with the moments in Eqs. (30) and (31), both on a surface of length $L = 40$. The quality of the agreement between the two solutions shows that the Langevin equation correctly describes the time scale of the relaxation toward equilibrium. This result is especially important for modelling other equilibration processes such as Ostwald ripening, the recovery phase of epitaxial growth, and the decay of nanostructures on surfaces.

VIII. DISCUSSION

In the preceding sections, we have derived Langevin equations for several standard models of epitaxial growth. Our analytic description embodies the statistical information obtained from KMC simulations, but complements the purely algorithmic approach of the KMC method. This has several useful conceptual and practical consequences. For deposition models, where the correlation matrix is diagonal, the numerical integration of the Langevin equation provides a computational alternative to KMC simulations. But even in the presence of surface diffusion, which produces a correlation matrix with off-diagonal entries, an analytic formulation offers advantages because not all stochastic processes necessarily contribute equally to this matrix. For example, in the early stages of irreversible growth on a singular surface under typical operating conditions, nucleation is the most important stochastic process; all other processes, including deposition, can be taken as deterministic [69]. At later stages, as the surface roughens, surface diffusion is less

effective and the shot noise of the deposition becomes the dominant stochastic process [4]. Our analytic expression for the correlation matrix of the noise could provide the basis for an adaptive approach to stochastic integration or some other form of noise reduction [25].

The model described in Sec. VII provides a basic description of growth by molecular-beam epitaxy and has been used to explain many fundamental experimental observations [3, 35–37]. But it is for applications to heteroepitaxial systems, especially the theory of quantum dot formation, where establishing a Langevin equation is of prime importance. Equations of motion for heteroepitaxial morphology based on classical linear elasticity [71–73] have already met with considerable success, but such approaches cannot easily draw connections to atomistic processes. Although continuum elasticity can be derived by coarse-graining "ball-and-spring" models [74], and hybrid methods are now capable of determining the mesoscopic consequences of atomistic interactions [75, 76], a complete understanding of heteroepitaxial morphological evolution, particularly comparisons with specific materials systems, must await a more systematic treatment of the coarse-graining of atomic-scale kinetics in the presence of strain. Lattice-based models that subsume nonlocal elastic effects into local hopping barriers provide a useful starting point for such efforts.

Our approach is suitable for other lattice models with transition rules that fulfill the small jump and smoothness conditions in Sec. III, including the random walk with exclusion [77], which is a lattice realization of Burgers' equation, and ballistic deposition [78], which belongs to the Kardar-Parisi-Zhang (KPZ) universality class [4]. Sandpile models of self-organized criticality might be amenable to our method. An issue of considerable recent interest in this area is the relation between sandpile models and the depinning transition in quenched random media [79]. Phenomenological equations have been proposed for self-organized criticality [80], but systematic derivations are now beginning to appear [81]. Taking a broader view, epidemiology and population dynamics could also benefit from our analysis [82] and, indeed, a method similar to that developed here has been applied to population dynamics [83], albeit without spatially-dependent variables.

The wider significance of our method derives from the Langevin equation providing a starting point for the passage to the continuum limit. This can be carried out for the Edwards-Wilkinson model by transforming to coarse-grained variables based on "naive" scaling [50], but for models where such arguments fail, renormalization-group (RG) methods must be used. In this case, the regularized Langevin equation provides the initial condition for the RG and the subsequent trajectory determines any crossover regimes along the path to the stable fixed point. This establishes the basis for identifying the appropriate continuum equation as a function of coarse graining. Quite apart from the conceptual impact of this procedure, there are practical applications. A Langevin equation derived from first principles can be compared with equations derived from the statistics of growing surfaces to obtain estimates of fundamental parameters [84]. The comparison between the morphological evolution of real systems with predictions based on stochastic growth equations remains an active research area [85, 86] and our methodology is poised to contribute to this effort.

IX. SUMMARY AND CONCLUSIONS

We have derived Langevin equations for fluctuating surfaces that embody the statistical properties of KMC simulations. The statistical equivalence of the Langevin equation and the Chapman-Kolmogorov equation, as required by the Kurtz theorem [45–47], has been demonstrated with applications to several standard models. We have identified the important implementational issues of our method: the optimal regularization of the step functions used to characterize the local environment for a particular model, and the convergence of the Langevin to the KMC solution with increasing largeness parameter Ω. The convergence is slowest at the earliest times for the roughness and the smallest distances for the correlation function, where atomistic effects are most evident. But for longer times and larger distances on large lattices, even $\Omega = 1$ can provide a reliable account of the scaling behavior of correlation functions.

The availability of an exact analytic formulation of stochastic lattice models of growth provides a starting point for coarse-graining Langevin equations for input to RG transformations. This provides the basis for a first-principles continuum description of lattice models that would explain several intriguing observations of KMC simulations [24, 26–28] that as yet have no analytic justification. Finally, in the arena of heteroepitaxial phenomena, our method provides an opportunity to derive continuum equations whose coefficients retain their atomistic ancestry. This would pave the way towards a systematic approach to modelling heteroepitaxial growth for specific materials systems.

Acknowledgments

This work was supported by funds from the U.K. Engineering and Physical Sciences Research Council and the European Commission Sixth Framework Programme as part of the European Science Foundation EUROCORES Programme on Self-Organized Nanostructures (SONS).

APPENDIX A: STEP FUNCTION REGULARIZATION

The step functions in the transition rules that appear in the Chapman-Kolmogorov equation survive the passage to the Langevin equation, albeit as regularized func-

tions. However, the transition rules fix the step function $\theta(x)$ in Eq. (13) only for integer values of x [Fig. 10(a)]. The continuation of the step function to all real arguments must maintain the transition rules for continuous heights. This is a stringent condition on the regularization and depends on the rules of the model. An inappropriate choice of regularization can provide results that appear to be at variance with the Kurtz theorem, when it actually represents an inadvertent change of the model itself. The simplest regularization of $\theta(x)$ that fulfills the requirement of continuity discussed in Sec. III B is

$$\theta(x;a) = \frac{1}{a}\left[\max(x+a,0) - \max(x,0)\right] , \qquad \text{(A1)}$$

where $0 < a \leq 1$ and $\max(x,y)$ is the greater of x and y. The general form of this regularization is shown in Fig. 10(b). No other regularizations we have constructed has produced superior results to those based on Eq. (A1).

1. The Edwards-Wilkinson Model

The transition rates of the Edwards-Wilkinson model are based on identifying the minimum height(s) from among a randomly chosen site and its two nearest neighbors. Expressions for these transition rates are given in Eqs. (52)–(54). The rules of this model are extended to continuous variables by requiring that the height is *always* minimized, even if the height differences between neighboring sites are less than one unit.

Several typical local height configurations and their deposition probabilities obtained by using $\theta(x;1)$ and $\theta(x;0.01)$ in Eqs. (52)–(54) are shown in Fig. 11. These comparisons demonstrate the striking effect that different choices of regularization $\theta(x;a)$ have on the morphological evolution of a surface for nominally the same transition rules. We see that, apart from the configuration where the original site has the minimum height, $\theta(x;1)$ produces a bias toward *greater* heights than $\theta(x)$, which clearly violates the spirit of the Edwards-Wilkinson rules. Configurations in which the original site has the greatest height by less than one unit provide the most telling

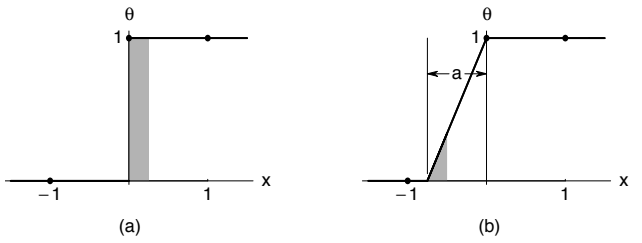

FIG. 10: (a) The step function in Eq. (13), and (b) the regularization in Eq. (A1). The function in (b) has the same values for integer arguments, which are indicated by dots, as the function in (a) for $0 < a \leq 1$. The shaded regions show how the abrupt threshold behavior in (a) is smoothed by the regularization in (b).

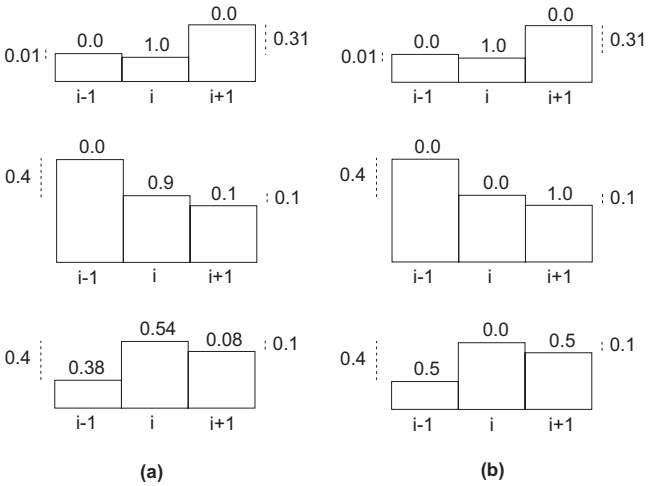

FIG. 11: Local deposition probabilities for the Edwards-Wilkinson model using (a) $\theta(x;1)$ and (b) $\theta(x;0.01)$, where $\theta(x;a)$ is defined in Eq. (A1). The randomly chosen site is denoted by i and the deposition probabilities to each site are written at the top of the corresponding column. Height differences between the central and nearest-neighbor heights are shown at the sides of each configuration.

difference: $\theta(x;1)$ actually favors this as the deposition site, again in violation of the Edwards-Wilkinson criterion. On the basis of these considerations, we expect that $\theta(x;1)$ produces a rougher surface than $\theta(x;0.01)$ and, more importantly, that $\theta(x;0.01)$ provides the more faithful extension of the Edwards-Wilkinson model to continuous variables.

Figure 12 compares the roughness calculated from the Langevin equation by using $\theta(x;1)$ and $\theta(x)$ with that obtained from KMC simulations. The regularization with $\theta(x;1)$ does indeed lead to a rougher surface than that

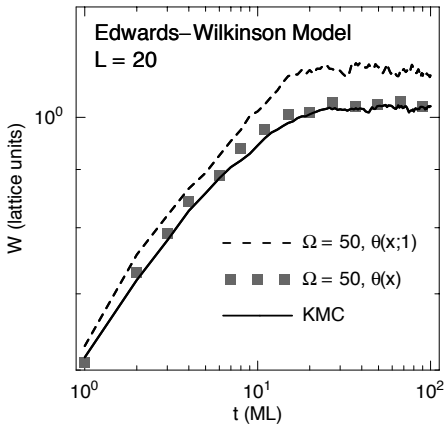

FIG. 12: The roughness in Eq. (44) for the Edwards-Wilkinson model obtained by solving the Langevin equation with $\Omega = 50$ for a system of size $L = 20$ using the regularization $\theta(x;1)$ defined in Eq. (A1) and the original threshold function $\theta(x)$ in Eq. (13). Each data set was obtained from an average of 1500 realizations.

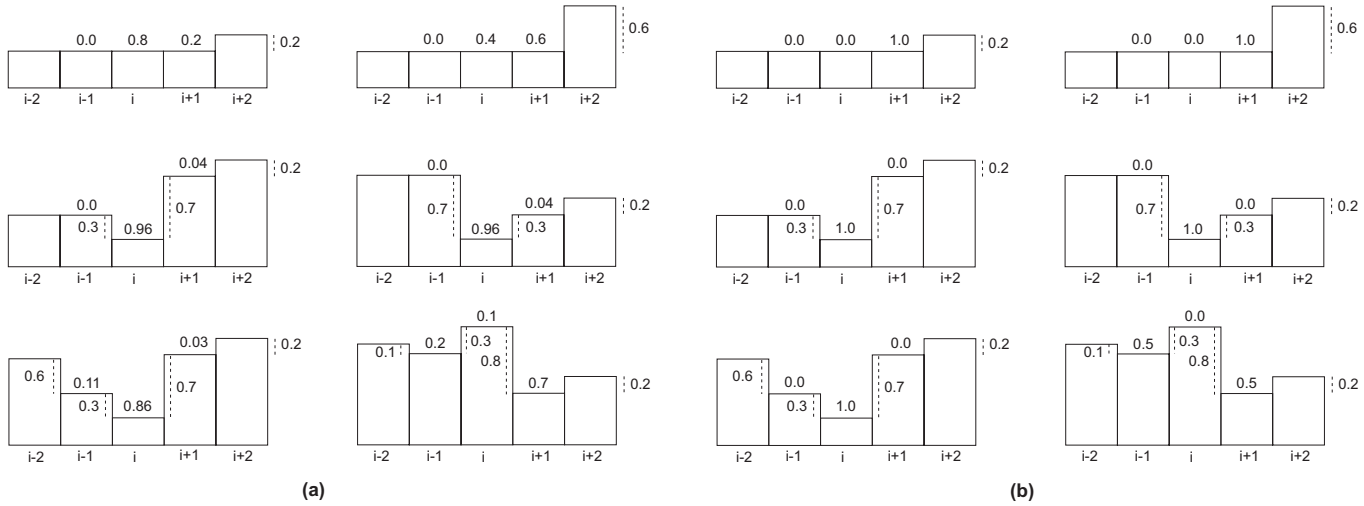

FIG. 13: Local deposition probabilities for the Wolf-Villain model using (a) $\theta(x;1)$ and (b) $\theta(x;0.01)$. The randomly chosen site is denoted by i and the transition probabilities to each site are written at the top of the corresponding column. Height differences between the central and nearest-neighbor heights are indicated at the sides of each configuration.

obtained from KMC simulations at all times. The two Langevin solutions yield approximately the same slope at pre-saturation times, but then begin to diverge, and show an appreciable difference in their saturation values. By contrast, the calculation with $\theta(x)$ agrees with the KMC roughness at all times. As this suggests, the Langevin solution with the regularizations $\theta(x;a)$ using decreasing values of a converges to the KMC solution as $a \to 0$. Thus, the optimal choice is, in fact, no regularization at all. Operationally, we can either choose a value of a small enough to produce agreement with KMC simulations to some prescribed tolerance, or simply take the limit $a \to 0$ after having performed the Kramers-Moyal-van Kampen expansion.

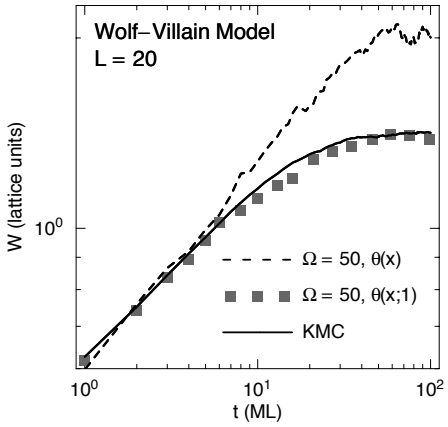

FIG. 14: The roughness in Eq. (44) for the Wolf-Villain model obtained by solving the Langevin equation with $\Omega = 50$ for a system of size $L = 20$ using $\theta(x;1)$ and $\theta(x)$. Each set of data was obtained from an average of 1500 realizations.

2. The Wolf-Villain Model

The deposition rules of the Wolf-Villain model are based on identifying the site that maximizes the number of nearest neighbors. The transition probabilities for several representative configurations are shown in Fig. 13. These have been calculated by using $\theta(x;1)$ and $\theta(x;0.01)$ in the local transition rates in Table I. An immediate consequence of the height variables becoming continuous is that the likelihood of nearest-neighbors having the same height is essentially zero. Consequently, configurations in Figs. 4 and 5 whose transitions rely on the equality of neighboring heights are effectively pre-empted by the sharp threshold function in Eq. (13). Therefore, for height differences lying in the range $[0,1]$, the rules of the Wolf-Villain model *must* be applied gradually, so we expect that $\theta(x;1)$ provides the optimal regularization for this model.

The four configurations shown in the top row of Fig. 13 illustrate the main difference between the two regularizations. The maximum coordination is identified as the deposition site by $\theta(x;0.01)$. However, with $\theta(x;1)$, there is a gradual transition of the most probable deposition site as the height of the second-nearest neighbor increases, which effectively increases the coordination of the nearest neighbor. For configurations where the initial site has the lowest height, both regularizations are in broad agreement if the height differences are large enough. The regularization $\theta(x;1)$ again yields appreciable probabilities onto neighboring sites if their coordination, as measured by neighboring height differences, is sufficient. This regularization allows deposition onto the initial site if neighboring sites have non-zero coordination, but correctly identifies the site with the greatest coordination, which $\theta(x;0.01)$ does not. In effect, $\theta(x;1)$ smears out small height differences.

The roughness calculated from the Langevin equation with both regularizations is compared in Fig. 14 with the KMC roughness. The regularization $\theta(x; 0.01)$ produces a much greater saturation roughness and a delayed saturation time than $\theta(x; 1)$, although there is agreement at early times between all three solutions. For the Wolf-Villain model, therefore, $\theta(x; 1)$ is the more accurate regularization.

[1] A. Madhukar and S. V. Ghaisas, CRC Crit. Rev. Solid State Mater. Sci. **14**, 1 (1988).

[2] H. Metiu, Y.-T. Liu, and Z. Zhang, Science **255**, 1088 (1992).

[3] T. Shitara, D. D. Vvedensky, M. R. Wilby, J. Zhang, J. H. Neave, and B. A. Joyce, Phys. Rev. B **46**, 6815 (1992).

[4] A.-L. Barabási and H. E. Stanley, *Fractal Concepts in Surface Growth* (Cambridge University Press, Cambridge, England, 1995).

[5] T. Halpin-Healy and Y.-C. Chang, Phys. Rep. **254**, 215 (1995)

[6] J. Krug, Adv. Phys. **46**, 139 (1997).

[7] A. Pimpinelli and J. Villain, *Physics of Crystal Growth* (Cambridge University Press, Cambridge, England, 1999).

[8] I. V. Markov, *Crystal Growth for Beginners: Fundamentals of Nucleation, Crystal Growth and Epitaxy* 2nd edn (World Scientific, Singapore, 2003).

[9] J. Villain, J. Phys. I **1**, 19 (1991).

[10] Z. W. Lai and S. Das Sarma, Phys. Rev. Lett. **66**, 2348 (1991).

[11] M. Kardar, G. Parisi, and Y.-C. Zhang, Phys. Rev. Lett. **56**, 889 (1986).

[12] T. Hwa and M. Kardar, Phys. Rev. A **45**, 7002 (1992).

[13] M. Marsili, A. Maritan, F. Toigo, and J. R. Banavar, Rev. Mod. Phys. **68**, 963 (1996).

[14] S.-C. Park, D. Kim, and J.-M. Park, Phys. Rev. E **65**, 015102(R) (2001).

[15] C.-H. Lam and L. M. Sander, Phys. Rev. Lett. **71**, 561 (1993).

[16] Z. Rácz, M. Siegert, D. Liu, and M. Plischke, Phys. Rev. A **43**, 5275 (1991)

[17] D. D. Vvedensky, A. Zangwill, C. N. Luse, and M. R. Wilby, Phys. Rev. E **48**, 852 (1993).

[18] M. Předota and M. Kotrla, Phys. Rev. E **54**, 3933 (1996).

[19] G. Costanza, Phys. Rev. E **55**, 6501 (1997).

[20] F. Family, J. Phys. A **19**, L441 (1986).

[21] J. M. Kim and S. Das Sarma, Phys. Rev. Lett. **72**, 2903 (1994).

[22] M. R. Wilby, D. D. Vvedensky, and A. Zangwill, Phys. Rev. B **46**, R12896 (1992); **47**, 16068 (1993).

[23] J. Krug, M. Plischke, and M. Siegert, Phys. Rev. Lett. **70**, 3271 (1993).

[24] M. Kotrla and P. Šmilauer, Phys. Rev. B **53**, 13777 (1996).

[25] P. Punyindu and S. Das Sarma, Phys. Rev. E 57, R4863 (1998).

[26] S. Das Sarma, P. P. Chatraphorn, and Z. Toroczkai, Phys. Rev. E 65, 036144 (2002).

[27] S. Pal and D. P. Landau, Physica A **267**, 406 (1999).

[28] S. Pal, D. P. Landau, and K. Binder, Phys. Rev. E **68**, 021601 (2003).

[29] C. Baggio, R. Vardavas, D. D. Vvedensky, Phys. Rev. E **64**, 045103(R) (2001).

[30] S. F. Edwards and D. R. Wilkinson, Proc. R. Soc. London Ser. A **381**, 17 (1982).

[31] S. Clarke and D. D. Vvedensky, Phys. Rev. B **37**, R6559 (1988).

[32] D. E. Wolf and J. Villain, Europhys. Lett. **13**, 389 (1990).

[33] S. Das Sarma and P. Tamborenea, Phys. Rev. Lett. **66**, 325 (1991).

[34] C. M. Horowitz and E. V. Albano, J. Phys. A **34**, 357 (2001).

[35] M. C. Bartelt and J. W. Evans, Phys. Rev. B **46**, 12675 (1992).

[36] C. Ratsch, P. Šmilauer, A. Zangwill, and D. D. Vvedensky, Surf. Sci. **329**, L599 (1995).

[37] J. G. Amar and F. Family, Phys. Rev. Lett. **74**, 2066 (1995).

[38] M. D. Johnson, C. Orme, A. W. Hunt, D. Graff, J. Sudijono, L. M. Sander, and B. G. Orr, Phys. Rev. Lett. **72**, 116 (1994).

[39] P. Šmilauer and D. D. Vvedensky, Phys. Rev. B **52**, 14263 (1995).

[40] M. Itoh, G. R. Bell, A. R. Avery, T. S. Jones, B. A. Joyce, and D. D. Vvedensky, Phys. Rev. Lett. **81**, 633 (1998).

[41] P. Kratzer and M. Scheffler, Phys. Rev. Lett. **88**, 036102 (2002).

[42] N. G. van Kampen, *Stochastic Processes in Physics and Chemistry* (North-Holland, Amsterdam, 1981).

[43] A. K. Myers–Beaghton and D. D. Vvedensky, Surf. Sci. **232**, 161 (1990).

[44] J. W. Evans and J. W. Evans, Phys. Rev. E **49**, 1061 (1994).

[45] T. G. Kurtz, Math. Prog. Stud. **5**, 67 (1976).

[46] T. G. Kurtz, Stoch. Proc. Appl. **6**, 223 (1978).

[47] R. F. Fox and J. Keizer, Phys. Rev. A **43**, 1709 (1991).

[48] J. Krug, P. Meakin, T. Halpin-Healy, Phys. Rev. A **45**, 638 (1992).

[49] E. Marinari, A. Pagnani, G. Parisi, and Z. Rácz, Phys. Rev. E **65**, 026136 (2002).

[50] D. D. Vvedensky, Phys. Rev. E **67**, 025102(R) (2003).

[51] D. D. Vvedensky, Phys. Rev. E **68**, 010601(R) (2003).

[52] P. Šmilauer, M. R. Wilby and D. D. Vvedensky, Phys. Rev. B **47**, R4119 (1993).

[53] M. Siegert and M. Plischke, Phys. Rev. E **50**, 917 (1994).

[54] A. Zangwill, *Physics at Surfaces* (Cambridge University Press, Cambridge, 1988).

[55] The Kramers-Moyal-van Kampen expansion in Eq. (18) is meaningful despite the fact that the moments of the transition rates contain threshold functions [e.g. Eq. (28)], which are not differentiable at vanishing argument. This problem is alleviated by replacing these functions with smooth approximations [50], which can be done to arbitrary accuracy, and then restoring the original threshold functions in the Langevin equations.

[56] Fox and Keizer [47] refer to this as Kurtz's *second* theorem.

[57] J. L. Doob, Ann. Math. **43**, 351 (1942); Reprinted in *Noise and Stochastic Processes*, edited by N.Wax (Dover,

New York, 1954), pp. 319–337.
[58] J. F. Kenney and E. S. Keeping, *Mathematics of Statistics*, Part 2, 2nd edn. (Van Nostrand, Princeton, NJ, 1951), pp. 298–300.
[59] A. L.-S. Chua, *Mathematical Aspects of Epitaxial Systems*, Ph. D. thesis, (University of London, 2004, unpublished).
[60] M. Schroeder, M. Siegert, D. E. Wolf, J. D. Shore, and M. Plischke, Europhys. Lett. **24**, 563 (1993).
[61] K. Park, B. Kahng, and S. S. Kim, Physica A **210**, 146 (1994).
[62] P. Šmilauer and M. Kotrla, Phys. Rev. B **49**, R5769 (1994).
[63] C. S. Ryu and I. M. Kim, Phys. Rev. E **51**, 3069 (1995); **52**, 2424 (1995).
[64] E. Medina, T. Hwa, M. Kardar, and Y.-C. Zhang, Phys. Rev. A **39**, 3053 (1989).
[65] Z.-F. Huang and B.-L. Gu, Phys. Rev. E **54**, 5935 (1996).
[66] G. Costanza, J. Phys. A **31**, 7211 (1998).
[67] C. Herring, in *The Physics of Powder Metallurgy*, edited by W. E. Kingston (McGraw-Hill, New York, 1951), pp. 143-179.
[68] W. W. Mullins, J. Appl. Phys. **28**, 333 (1957).
[69] C. Ratsch, M. F. Gyure, S. Chen, M. Kang, and D. D. Vvedensky, Phys. Rev. B **61**, R10598 (2000).
[70] P. I. Tamborenea and S. Das Sarma, Phys. Rev. E **48**, 2575 (1993).
[71] B. J. Spencer, P. W. Voorhees, and S. H. Davis, J. Appl. Phys. **73**, 4955 (1993).
[72] B. J. Spencer, S. H. Davis, and P. W. Voorhees, Phys. Rev. B **47**, 9760 (1993).
[73] A. A. Golovin, S. H. Davis, and P. W. Voorhees Phys. Rev. E **68** (2003) 056203.
[74] Y. Saito, H. Uemura, and M. Uwaha, Phys. Rev. B **63**, 045422 (2001).
[75] A. C. Schindler, M. F. Gyure, G. D. Simms, D. D. Vvedensky, R. E. Caflisch, C. Connell, and E. Luo, Phys. Rev. B **67**, 075316 (2003).
[76] W. A. Curtin and R. E. Miller, Modelling Simul. Mater. Sci. Eng. **11** R33 (2003).
[77] C. Haselwandter and D. D. Vvedensky, J. Phys. A **35**, L579 (2002).
[78] C. A. Haselwandter and D. D. Vvedensky, in *Modeling of Morphological Evolution at Surfaces and Interfaces*, edited by J. Evans, C. Orme, M. Asta, and Z. Zhang, Mat. Res. Soc. Symp. Proc. **859E** (Materials Research Society, Pittsburgh, PA, 2005), pp. JJ8.8.1–JJ8.8.6.
[79] M. Paczuski and S. Boettcher, Phys. Rev. Lett. **77**, 111 (1996).
[80] E. T. Lu, Phys. Rev. Lett. **74**, 2511 (1995).
[81] G. Pruessner, Phys. Rev. E **67**, 030301(R) (2003).
[82] W.-Y. Chen and S. Bokka, J. Theor. Bio. **234**, 455 (2005).
[83] J. P. Aparicio and H. G. Solari, Phys. Rev. Lett. **86**, 4183 (2001).
[84] G. R. Jafari, S. M. Fazeli, F. Ghasemi, S. M. Vaez Allaei, M. R. Tabar, A. Iraji zad, and G. Kavei, Phys. Rev. Lett. **91**, 226101 (2003).
[85] A. Ballestad, B. J. Ruck, M. Adamcyk, T. Pinnington, and T. Tiedje, Phys. Rev. Lett. **86**, 2377 (2001).
[86] H.-C. Kan, S. Shah, T. Tadyyon-Eslami, and R. J. Phaneuf, Phys. Rev. Lett. **92**, 146101 (2004).